Computers in Biology and Medicine 104 (2019) 197–204

Contents lists available at ScienceDirect

Computers in Biology and Medicine

journal homepage: www.elsevier.com/locate/compbiomed

Intraventricular blood flow with a fully dynamic mitral valve model

Seyed Saeid Khalafvand[a,*], Fei Xu[a], Jos Westenberg[b], Frank Gijsen[c], Sasa Kenjeres[a]

[a] Department of Chemical Engineering, Faculty of Applied Science, Delft University of Technology, the Netherlands
[b] Department of Radiology, Leiden University of Medical Center, Leiden, the Netherlands
[c] Department of Biomedical Engineering, Thorax Center, Erasmus MC, Rotterdam, the Netherlands

ARTICLE INFO

Keywords:
Blood flow
Mitral valve
Left ventricle
Boundary value problem
Vortices
Dynamic mesh
CFD

ABSTRACT

Mitral valve (MV) leaflets affect the formation, growth, and decay of vortices in the left ventricle (LV) during diastolic filling. The shape and motion of MV leaflets are simplified in most studies due to computational restrictions. In this study, we present a newly developed mathematical method to model the dynamic movement of valve leaflets and annulus, which is based on *in vivo* data obtained with magnetic resonance imaging (MRI). In the present method, we solve a boundary value problem where the MV surface is initially unknown. The resultant MV shapes are included in a dynamic motion model of the LV to assess the change of intraventricular flow patterns. To estimate the effects of the MV on left intraventricular flow, a LV model without MV leaflets was also simulated for comparison. Our study showed that the presence of the MV and the shape of its leaflets significantly altered the formation and evolution of vortex structures in the LV. The various MV leaflet shapes accelerate the transvalvular flow distinctly, leading to different formation and development of vortex structures.

1. Introduction

It has been shown that the mitral valve (MV) affects the vortex formation and its motion inside the left ventricle (LV) during diastolic phase [1–4]. The MV shape is asymmetric regarding leaflets (anterior and posterior) and annulus. The complex structure of the MV and its severe deformation during opening and closing impose tremendous challenges in the numerical simulations. The 2D numerical models were employed to study the LV with rigid leaflets, which motion was solved using Fluid-Structure Interaction (FSI) approach [5,6] or derived from cardiovascular magnetic resonance (CMR) images along the long-axis view [1]. Despite the limitation of 2D modeling, these studies demonstrated the formation of a pair of vortices (i.e., cross-sections of a vortex ring in 3D) at the tips of the MV leaflets. To have a better understanding of the effects of MV on vortex formation in 3D ventricle flow, various attempts have been made. In Ref. [7]; the MV was modeled as an obstacle, and it opened at a fixed angle during entire diastole, while neglecting leaflet dynamics. In Ref. [3]; the MV was based on physiological data, and its motion was measured from a separate echocardiographic scan. They hinged the MV at a fixed semi-circular mitral annulus, and curvature effects of leaflets in flow direction were ignored. To model the interaction between ventricular flow and the MV, FSI was applied by Ref. [8]; though the coupling between the LV and MV were significantly simplified with only one degree of freedom. Most recently [4], modeled the MV motion based on a CMR scan in long-axis view. They prescribed the motion of the simplified MV assuming the anterior and posterior leaflets to be semi-cylindrical (truncated-cone) based on a rigid mitral annulus.

The present study is focused on a mathematical model of fully dynamic valve leaflets motion coupling with LV motion. We have developed a surface grid generation code based on opening angles and MV boundaries, enabling us to model the deformation of leaflets during opening and closing. Moreover, the longitudinal and radial movement of the mitral annulus will be included in the simulations. By solving a boundary value problem, the initial unknown MV surface will be determined. For this study, we have improved previous methods (rigid body and prescribed motion by interpolation) and we will show that the main advantage of this method is that the MV surface has its full deformation during the cardiac cycle.

2. Methods

2.1. Geometry reconstruction

The geometry used is based on a 4-D statistical shape model (SSM) generated from the dataset of 150 subjects, and includes the left ventricle, atrium, and aorta, as described in more details in Refs. [9,10]. The surface geometry is represented by polygonal mesh containing

* Corresponding author. Faculty of Applied Sciences, Delft University of Technology Delft, the Netherlands.
E-mail address: s.s.khalafvand@tudelft.nl (S.S. Khalafvand).

https://doi.org/10.1016/j.compbiomed.2018.11.024
Received 13 September 2018; Received in revised form 27 November 2018; Accepted 28 November 2018
0010-4825/

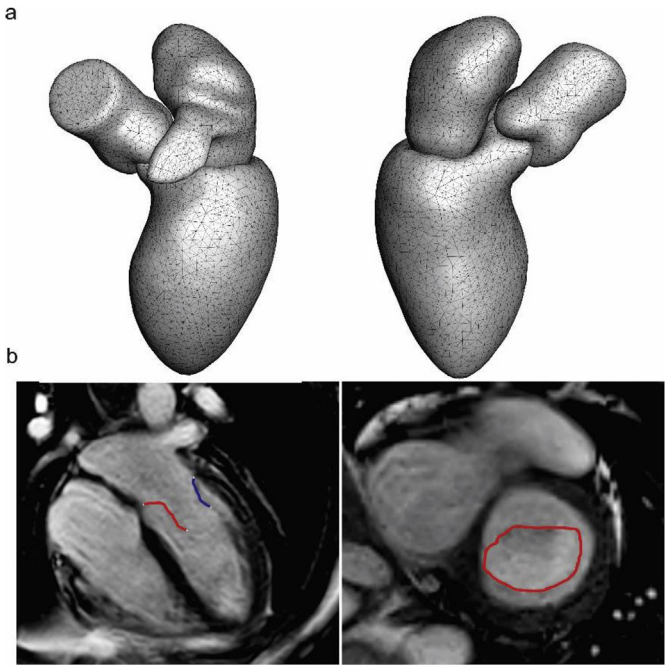

Fig. 1. (a) Geometries of LV, left atrium and aortic root in two different views. (b) 4 chamber long axis and short axis MV leaflet and annulus contours.

5170 vertices, which are further adjusted by applying interpolation for each of 20 time instants per single cardiac cycle. The example of the mean shape of the used geometry (two different views) is shown in Fig. 1a.

CMR was performed on a 3T MRI scanner (Ingenia, Philips Medical Systems, The Netherlands) with maximal amplitude of 45 mT/m for each axis, slew rate of 200 T/m/s and a combination of FlexCoverage Posterior coil in the table top with a dStream Torso coil, providing up to 32 coil elements for signal reception. Cine two-dimensional (2D) left 2-chamber, 4-chamber, and a cine multi-2D short-axis stack of slices were acquired, using steady-state free-precession (SSFP) sequences with echo time 1.5 ms, repetition time 3.0 ms, 350 mm field-of-view, 45° flip angle, acquisition resolution $1.9 \times 2.0 \times 8.0\ mm^3$. Retrospective gating was used with 30 phases reconstructed to represent one cardiac cycle. Breath holding was performed. Contours of the valve leaflets were manually delineated by one observer (JJMW) with over 20 years of experience in MRI, using in-house developed MASS software. MRI of a 47 years old healthy volunteer man was used in this study. The acquisition was part of a study protocol which was approved by the local Medical Ethical Committee of the Leiden University Medical Centre and informed consent was obtained. A view of the MV leaflets and annulus in 4-chamber and short-axis planes is depicted in Fig. 1b.

2.2. Mitral valve model

The motion of the two leaflets is defined by the opening angles α and β (see Fig. 2a). During the motion, the opening angles are prescribed, and the tips of the leaflets will move accordingly. Using opening angles and the initial leaflets shapes with a fixed annulus, one can generate the MV motion during the cardiac cycle by using interpolation or CAD software (a rigid motion). However, it is important to model the full dynamics of the valve deformation during opening and closing. The shape of anterior leaflet deforms during the cardiac cycle and its distortion is more complicated than the posterior leaflet. The posterior leaflet preserves its convex shape during the cardiac cycle. However, the anterior leaflet has a convex-concave shape during opening. In addition to leaflets shapes deformation, the MV annulus has also an upward/downward and contraction/dilation motions during the cardiac cycle.

To include all of this motions and deformations, we have developed a surface grid generation code which works based on opening angles and MV boundaries (annulus and commissures). To define the boundary of MV annulus, series of nodes were selected on the LV geometry (see the red dots in Fig. 2b) based on the patient data of the mitral valve defining MV annulus. Then we set the edge for anterior and posterior leaflets (see the green dots in Fig. 2b). After defining MV annulus, commissures and coaptation edges, a surface grid generation code is developed using elliptical equations to describe the motion of all surface nodes during opening and closing. For this purpose, the Poisson equation was used.

To implement such method, we create the surface (MV) differently from previous work which takes the surface as an interpolation from the boundary by using CAD software [4]. In our method, the surface (MV) is considered as the solution of a corresponding boundary value problem (BVP) in which the coordinates of the nodes on the MV surface are unknowns and the provided surface (MV) boundaries are taken as the boundary conditions for the BVP. With this transformation, the elliptical equations can be utilized to achieve the smooth surface. The general equations with boundary condition for the BVP are:

$$\left.\begin{aligned} \frac{\partial^2 X^{n+1}}{\partial x^2}+\frac{\partial^2 X^{n+1}}{\partial y^2}+\frac{\partial^2 X^{n+1}}{\partial z^2}&=f_X\\ \frac{\partial^2 Y^{n+1}}{\partial x^2}+\frac{\partial^2 Y^{n+1}}{\partial y^2}+\frac{\partial^2 Y^{n+1}}{\partial z^2}&=f_Y\\ \frac{\partial^2 Z^{n+1}}{\partial x^2}+\frac{\partial^2 Z^{n+1}}{\partial y^2}+\frac{\partial^2 Z^{n+1}}{\partial z^2}&=f_Z \end{aligned}\right\} \text{in } \Omega \text{ bounded with } \partial\Omega \tag{1}$$

where X^{n+1} , Y^{n+1} and Z^{n+1} are the x, y, z coordinates of the nodes inside the boundary at frame n + 1; f_X, f_Y, f_Z are source terms. $\partial\Omega^n$ and $\partial\Omega^{n+1}$ denote the boundary of the three-dimensional surface domain at *(n)*th and *(n + 1)*th frames, respectively. By using this equation for grid generation, O-type grid (a structured grid which connects the beginning and the end of the grid and forms an O-shape) can be achieved (see Fig. 2c). The workflow of our method is briefly depicted in Fig. 2d. It should be mention that for generation of unstructured triangular and mesh, DistMesh is used (Fig. 2d) in our code. DistMesh is a MATLAB code for generation of unstructured triangular and tetrahedral meshes. The code is relatively simple, and the user is able to define a variety of geometric shapes, and desired mesh densities.

Fig. 2e shows the MV at fully open and closed positions. However, there is a small gap at the closed position to fulfill mass balance during the cardiac cycle. We use three different colored dots in the figure: the blue dots are on the boundary of anterior leaflet; red dots on are the boundary of posterior leaflet; the pink dots are on the common boundary of anterior and posterior leaflet. This figure is an illustration of the topology-keeping mesh motion procedure.

2.3. Governing equations

The numerical simulations of the blood flow in left ventricle (including both filling and ejection phase) are performed by solving discretized forms of the mass and momentum conservation equations within the finite-volume method employing the arbitrary Lagrangian-Eulerian (ALE) formulation. The final form of the integrated continuity equation for a control volume (V) with surface (S) is given as:

$$\frac{\partial}{\partial t}\int_V \rho dV+\int_S \rho(\vec{v}-\vec{v}_b)\cdot\vec{n}\,dS=0 \tag{2}$$

where $\vec{v}$ is the velocity vector, $\vec{v}_b$ the velocity on the boundary, $\vec{n}$ the normal vector and ρ the blood density. The momentum equation is

$$\int_V \frac{\partial}{\partial t}(\rho\vec{v})dV+\int_S \rho\vec{v}\,(\vec{v}-\vec{v}_b)\cdot\vec{n}\,dS=-\int_S p\mathbf{I}\cdot\vec{n}\,dS+\int_S \boldsymbol{\tau}\cdot\vec{n}\,dS \tag{3}$$

where p is the pressure, $\mathbf{I}$ the unit tensor, and $\boldsymbol{\tau}$ the viscous stress tensor. Blood flowing in large arteries can be treated as homogeneous

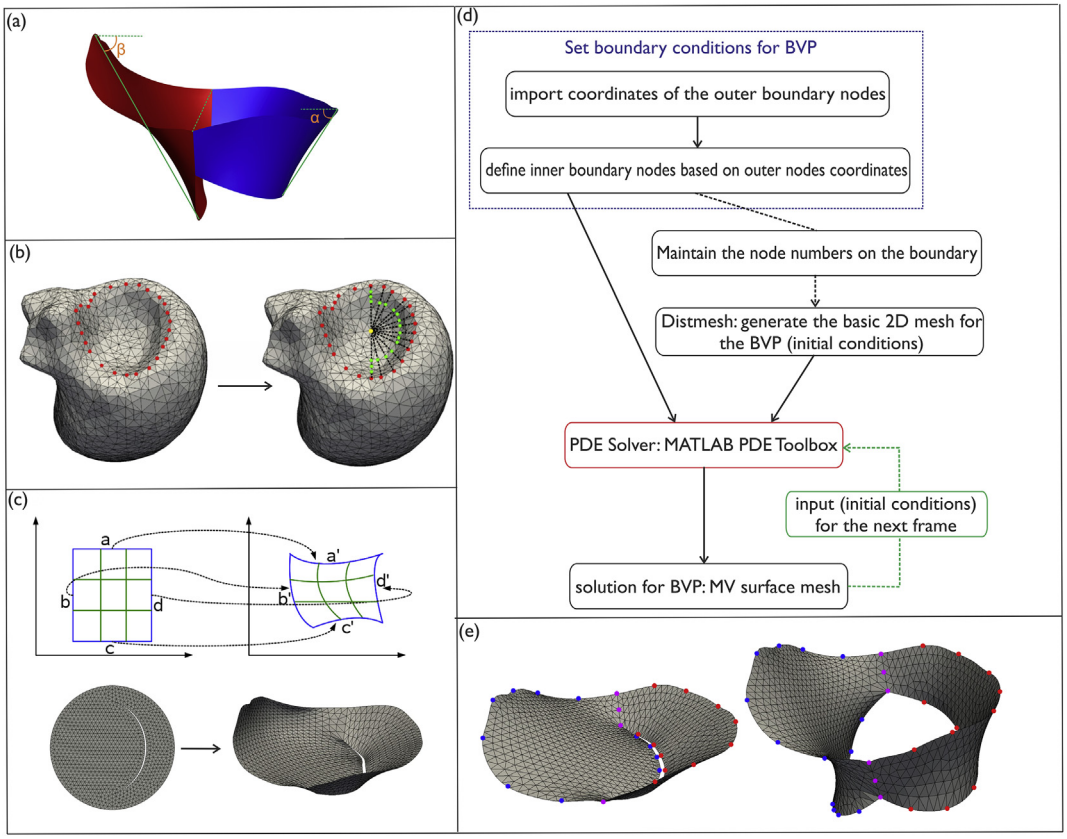

Fig. 2. (a) Opening angles of mitral valve leaflets. (b) Sketch map of the outer and inner boundary nodes. (c) A simple sketch of Grid generation method (d) Workflow of our approach to produce the MV surface mesh (e) Mitral valve model with colored dots for fully open and closed positions.

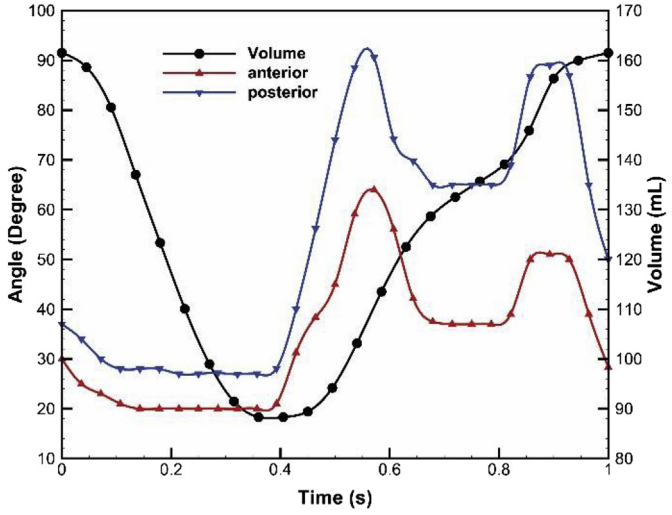

Fig. 3. Temporary change of LV volume, anterior and posterior leaflets opening angles during the cardiac cycle.

Newtonian fluid with density of 1050 kgm^{-3} and the dynamic viscosity of 0.00316$Pa\ s$. The periodic flow patterns are computed from an initial hydrostatic condition with the motion of the left ventricle and atrium, velocity at the atrial inlet for diastole, and no flow at the aortic outlet. During systole, velocity is prescribed at the outlet with no flow at the atrial inlet. The Navier-Stokes equations are solved using the finite volume CFD solver ANSYS Fluent (version 17.2). The motion of ventricle and valve leaflets are implemented through the user-defined functions (UDFs). The grid quality is monitored by the face skew angle below 40°, and the re-meshing software in ANSYS Fluent is applied when the grid quality needs to be improved. The final grid consists of approximately 12 million tetrahedral cells for the LV with MV leaflets. The PISO (pressure implicit with splitting of operators) algorithm [11] is employed along with a second order upwind scheme. The details of our numerical method have been described in our previous studies [9,12,13].

2.4. Vortex visualization

To capture and identify the most salient blood flow features inside the left ventricle, we apply so-called Q-criterion, which is based on calculation of the second invariant of the velocity gradient tensor [14]. This criterion enables us to extract the flow regions where the vorticity magnitude is greater than the strain magnitude (i.e. where $Q > 0$), which gives an indication of the vortex core. In the present study we adopt the identification threshold of $Q = 1000\ s^{-2}$ that is kept constant for comparative assessment of the obtained flow changes during pre-selected time instants of the cardiac cycle.

3. Results and discussion

3.1. Opening angles and volume change

Fig. 3 shows temporal change of LV volume, anterior and posterior leaflets opening angles during a cardiac cycle. The opening angles derived from MRI data are well synchronized with the change of LV volume. In this study, we have modeled the full cardiac cycle, and the motion of the closed MV is also considered.

3.2. Mitral valve model

The surface grid generated from our code is depicted in Fig. 4. It

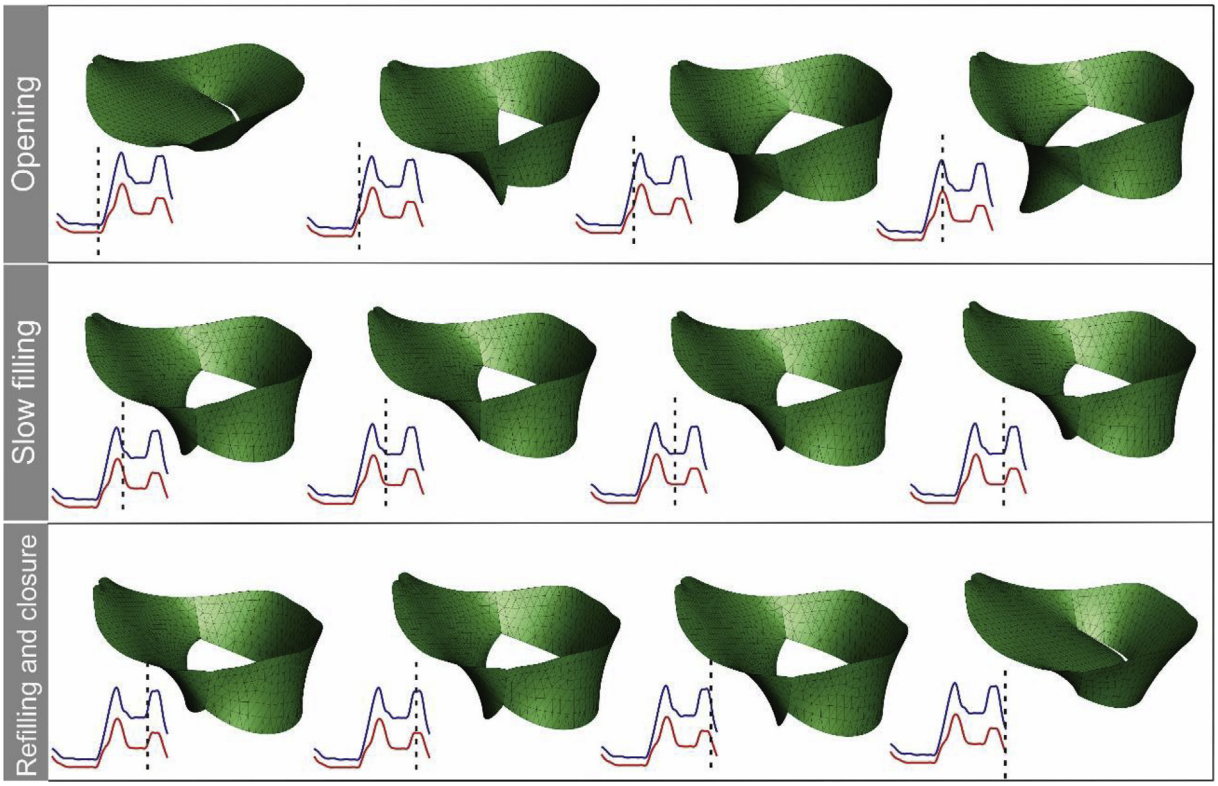

Fig. 4. The surface grid generated for MV leaflets with $f = 0$ during a cardiac cycle. Red and blue graphs show opening angles for anterior and posterior leaflets, respectively.

shows fully dynamic valve leaflets model produced by $f = 0$ in Eq. (1) at the initial opening to fully open (early filling), slow filling (diastasis) and refilling (late filling) and closure phases, respectively.

To assess the effects of the source term in Eq. (1) on MV leaflets shapes, two different source terms have been used: $f = +400$ and $f = -400$. As can be seen in Fig. 5, the positive source terms create a convex shape for anterior leaflet and concave shape for posterior, and *vice versa* for negative source terms. In this study, the normal mitral valve derived from healthy volunteer data is presented by $f = 0$. We have adjusted the boundary conditions in Eq. (1) with $f = 0$ to fit the MRI data for normal MV leaflet curvatures.

3.3. Diastolic flow patterns

The vortex structures during the initial rapid filling phase at three characteristic time instants (t = 0.045, 0.135 and 0.27 s) are plotted in Fig. 6. The creation and de-attachment of an asymmetric vortex ring caused by opening of the mitral valve is clearly observed. The initial radial extension of the vortex ring is determined by the size of cross-section of the MV opening. Similarly, the vortex ring orientation (defined as the angle between the vortex centre-of –axis and central vertical axis of LV) is determined by opening angles of MV leaflets. It can also be observed that initial asymmetry in vortex ring is caused by higher momentum in the proximity of the anterior leaflet.

Fig. 7 shows vortex structure during slow filling and re-filling. More vortices are generated for momentum balance during slow filling when inlet velocity reduces. Although the inflow decreases drastically, velocities in the ventricle do not, reflecting small viscous effect in this rapid flow deceleration phase.

The generation of the second vortex ring at the tip of mitral leaflets takes place, as can be seen in Fig. 7 (t = 0.405 s). The initial momentum of the first vortex ring provides a deeper penetration within the left ventricle (as seen at t-0.45s). After closing of the MV opening (at the end of diastole, t = 0.54 s), the breakup of the vortex rings takes place.

3.4. Systolic flow patterns

The vortex structures during the iso-volumetric contraction (IVC) are shown in Fig. 8. It can be seen that imposed momentum of LV contraction does not affect much behavior of the vortical structures (t = 0.585 s). When aortic valve opens, an ejecting jet is generated that starts to attract the vortex rings from the central part of LV (t = 0.675 s). With further contraction, this ejecting jet becomes stronger and vortex rings in the central interior of ventricle continue to desintegrate (t = 0.81 and 1 s). For a global overview of the temporal evolution of the flow field and corresponding vortical structures in the left ventricle, please see provided animation (provided as supplementary data 1).

3.5. Comparison

Fig. 9 compares vortex structure obtained from two different source terms in Eq (1), one with $f = 0$ and the other with $f = +400$. As prescribed in previous section $f = 0$ is calibrated for the normal MV derived from MRI. In addition, we have used $f = +400$ to show different curvatures of the MV leaflets as shown in Fig. 5. All simulation conditions were the same for both cases except the shape of the mitral valve. To demonstrate the effects of the MV, they are compared to a simulation for a LV without valve. In this simulation, only an effective open area was used as an orifice with no leaflets. They are shown in four significant points during filling phase: the peak of rapid filling (E-peak), deceleration, the peak of refilling (A-peak) and end-diastole.

In the simulation without valve, the initial vortex ring keeps its structure moving towards apex and a second vortex ring is produced during refilling - as was reported in our previous studies [1,12] and by others [15–17]. The large opening area of mitral orifice allowed the

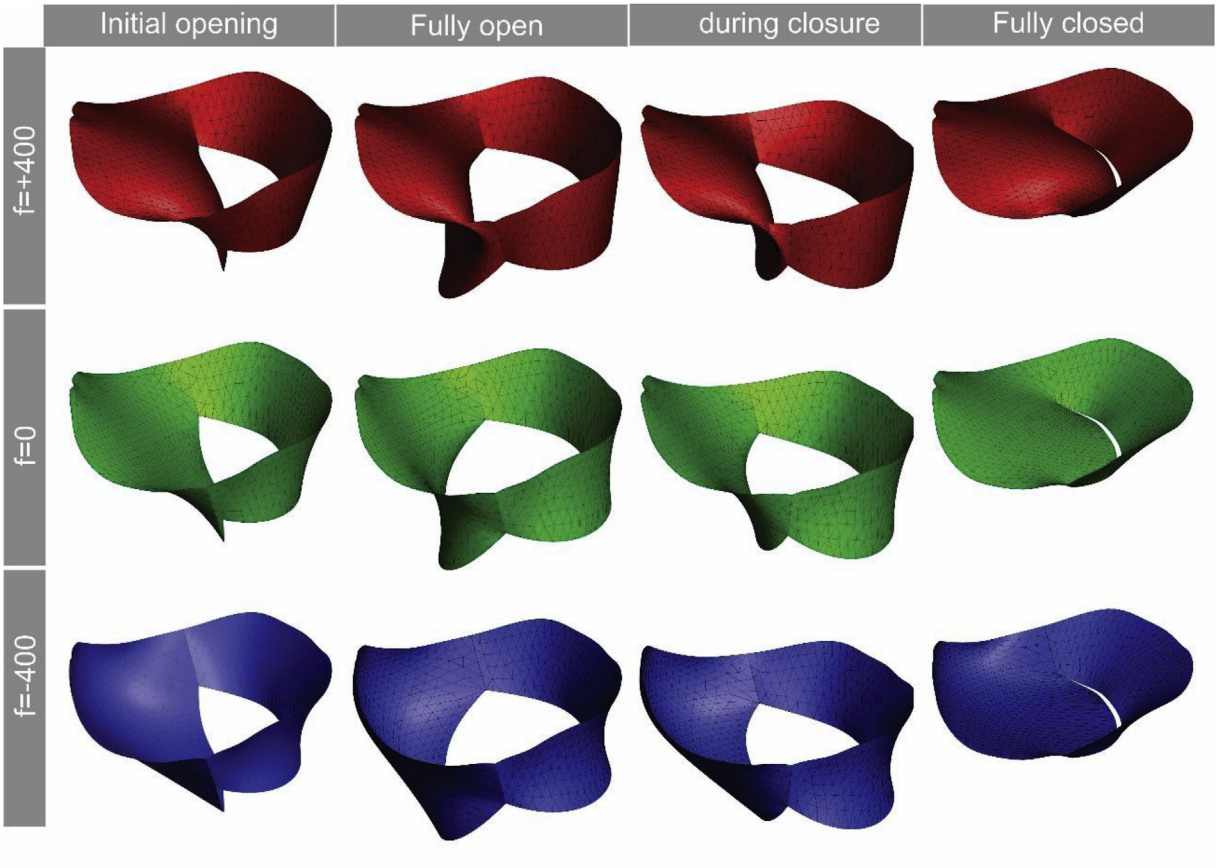

Fig. 5. Comparison of MV surface grid generated for $f = +400, 0, -400$ at four time instants.

transportation of vortices into LV without much dissipation. Thus, the flow field in LV was dominated by these vortices, especially during the rapid filling phase. Therefore, the simulation of physiological left heart without MV could not produce reasonable intraventricular flow.

In the presence of MV leaflets, vortex structures are more complicated as described in previous sections. The importance of incorporating MV leaflet dynamics into the flow field in the LV has been analyzed in present and other recent studies [1,3,4]. As can be seen in Fig. 9, the propagation of vortex ring to the apex for the simulation with valve is different from the simulation without valve. In a valvular model, the boundary layer separation occurred at the MV tips and the resultant vortex ring was initiated at the onset of the rapid filling phase. In addition, the wake of MV promoted the growth of vortex ring in size, which was further propelled towards the apex by the stronger transvalvular flow induced by the smaller effective opening area of MV. The asymmetric configuration of MV also plays a key role in the dominant direction of intraventricular flow, because the longer anterior leaflet directs the flow towards the lateral side of the LV wall.

The shape of the mitral valve leaflets in simulation is another important parameter of vortex formation and development as shown in this study. The comparison between two different source terms ($f = 0$ and $f = +400$) shows that the size, propagation, and location of vortex ring is different (Fig. 9). This indicates that the shape of the MV leaflets alters blood flow in LV. In most of the numerical studies, the effects of MV shape on left ventricular flow was ignored. Generally, the myocardium near the onset of diastolic is not much dilated with respect to the mitral orifice, and thus the vortex formation is delayed [13,18]. Consequently, the transvalvular flow through the larger mitral orifice

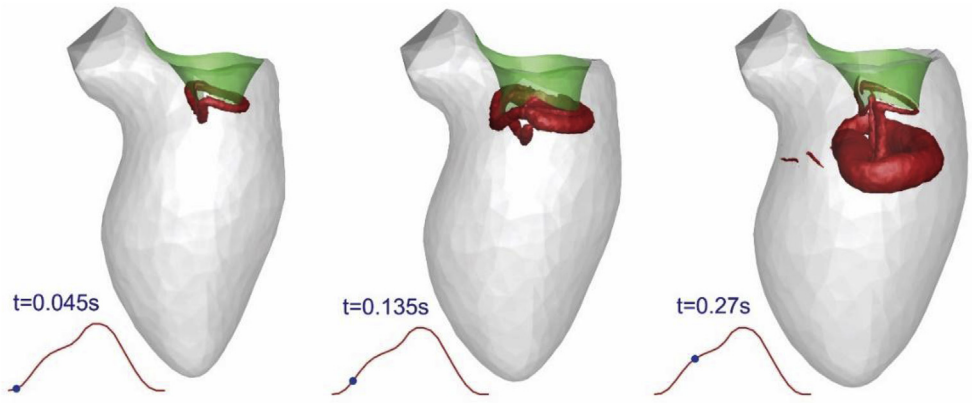

Fig. 6. Intraventricular vortex structures (Q-criterion = 1000) during rapid filling at three time instants.

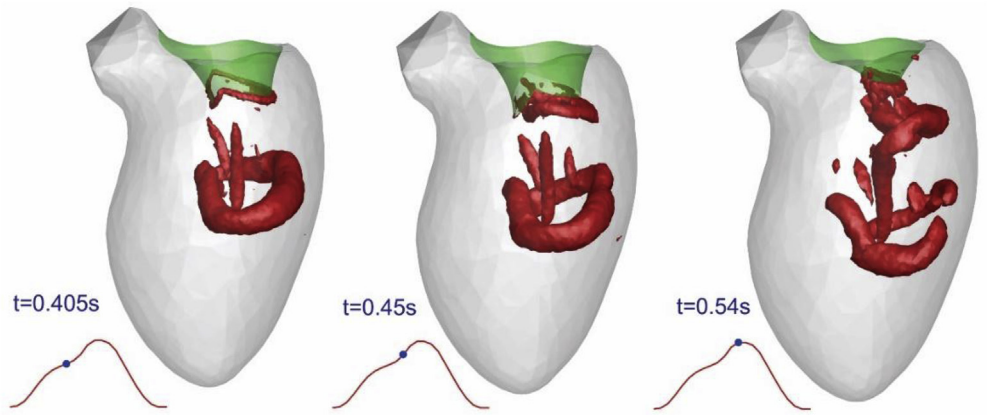

Fig. 7. Intraventricular vortex structures (Q-criterion = 1000) during slow filling and re-filling at three time instants.

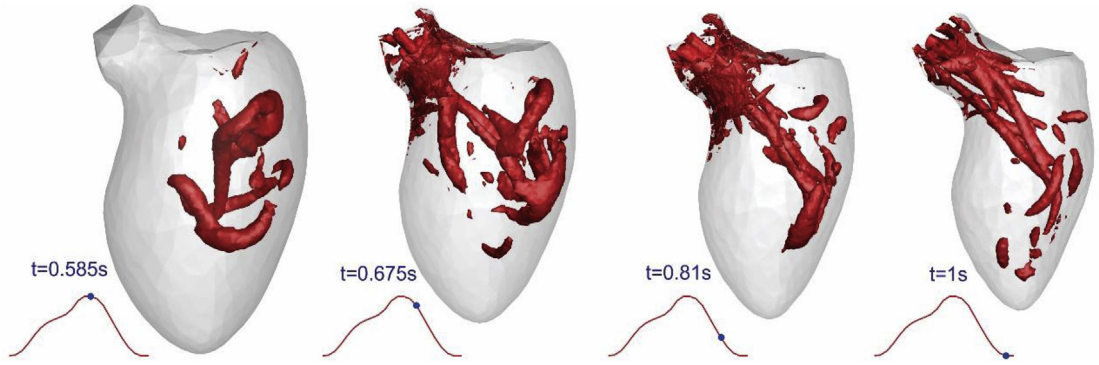

Fig. 8. Intraventricular vortex structures (Q-criterion = 1000) during IVC and systolic phase.

has lower momentum, leading to shorter propagation into LV chamber. In some studies, a purposely narrowed mitral orifice was adopted as a solution to facilitate vortex formation and mixture [19–21]. Despite the variation of the MV configuration, two vortex rings appear during the rapid filling and atrial contraction, respectively, which is also observed in another in-vivo study [22].

To quantify the effects of MV leaflets, the pressure difference between the MV annulus and apex is calculated. As depicted in Fig. 10, the pressure difference is higher for the LV with valve than without valve. The maximum pressure difference between $f = 0$ and valveless model is 223 Pa while between f = +400 and valveless model is 140 Pa. These comparisons show that the LV with MV leaflets creates the higher pressure difference and thus a better filling. In addition, the maximum pressure difference for two different source terms ($f = 0$ and $f = +400$) is 83 Pa (see Fig. 10).

3.6. Limitations

In this study, MRI data have been used to characterize MV shape and motion which are rather limited in terms of their spatial resolution. The 3D transoesophageal echocardiography (TOE) data can provide more accurate definition of motion and shape -especially for the MV. Note that here presented mathematical model of MV shape and motion can be easily adjusted to any other imaging method.

In present study, posterior leaflet is simplified due to limitations of the available MRI data. Typically, it consists of three cusps (P1, P2 and P3) and many pathologies are associated with specific cusps. However, the present method can provide more accurate results with an accurate input for posterior shape and motion.

Although we have used high order numerical schemes and fine grids, numerical errors can affect the results. The papillary muscles inside the LV are ignored. We assumed blood as a Newtonian fluid. In LV, average shear rate in the ventricle is high enough to justify the Newtonian assumption. However, the local shear rate in some areas such as apex is low.

4. Conclusion

In this study, we have developed an algorithm to produce a fully dynamic MV surface. Various MV leaflet surfaces were generated based on the same opening angles and MV annulus by changing the source term in our mathematical model. The shape models with an identical LV were modeled to estimate the effects of the MV with different source terms. The primary function of the MV is to ensure the unidirectional flow from left atrium to LV, which could not be granted in valveless models. Secondly, the MV accelerated transvalvular flow and promoted the growth of vortex ring in its wake, leading to farther propagation. Thirdly, its asymmetric configuration and different possible leaflets curvatures affect vortex formation and development in the LV. Otherwise, the flow direction would be largely influenced by the relative angle between the aortic root and left atrium. Lastly, the presentation of the fully dynamic model of the MV and its deformation during diastolic phase considerably changes the intraventricular flow. This observation implies that different MV leaflets shapes based on same data could produce different intraventricular flow.

Acknowledgments

This research is founded by The Netherlands Organization for Health Research and Development (ZonMW), within the project "4D Flow and Heart Failure", number 104003001.

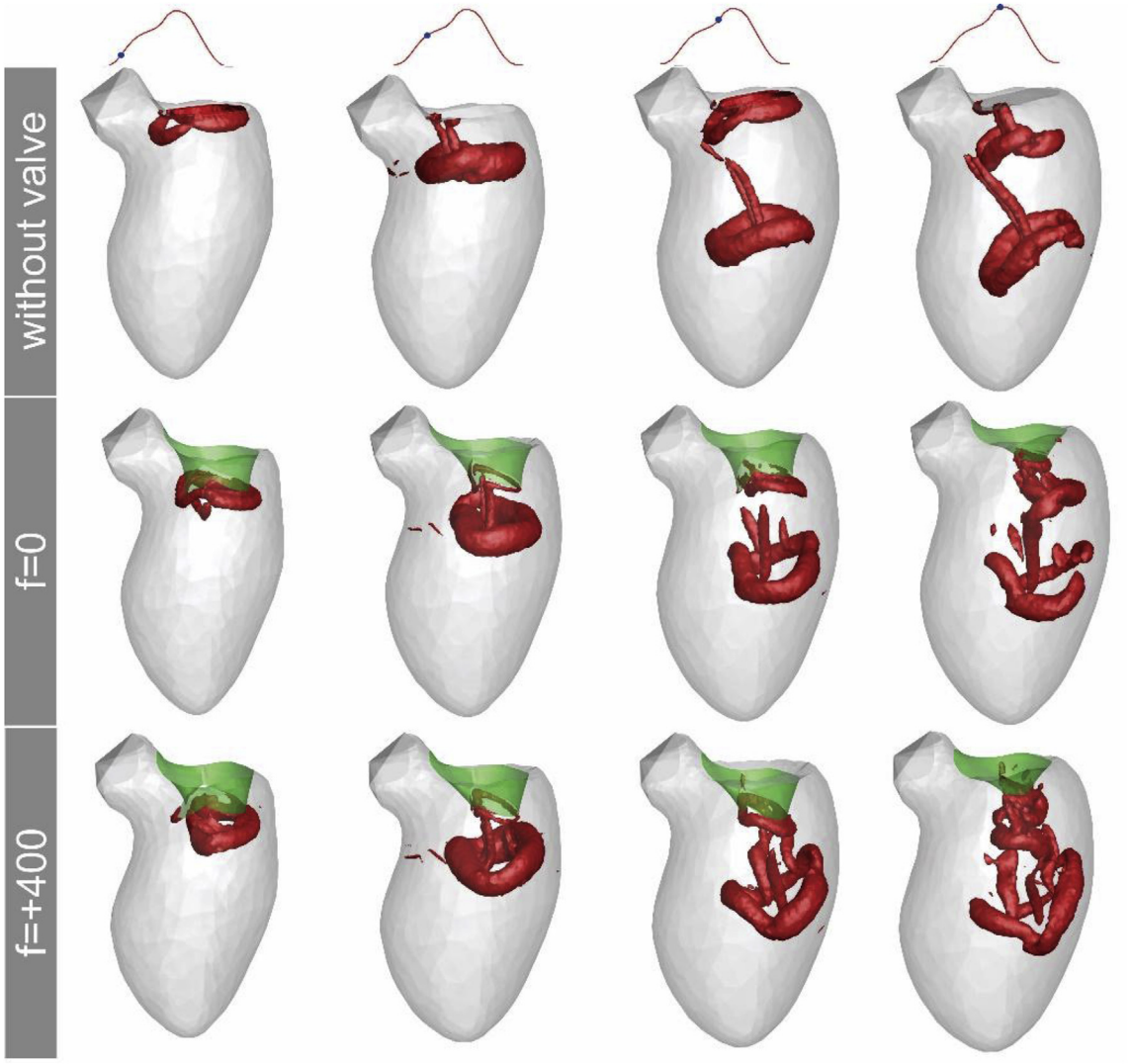

Fig. 9. Comparison of vortex structures (Q-criterion = 1000) during diastolic phase at four time instants for LV without valve and with valve ($f = 0$ and $f = +400$).

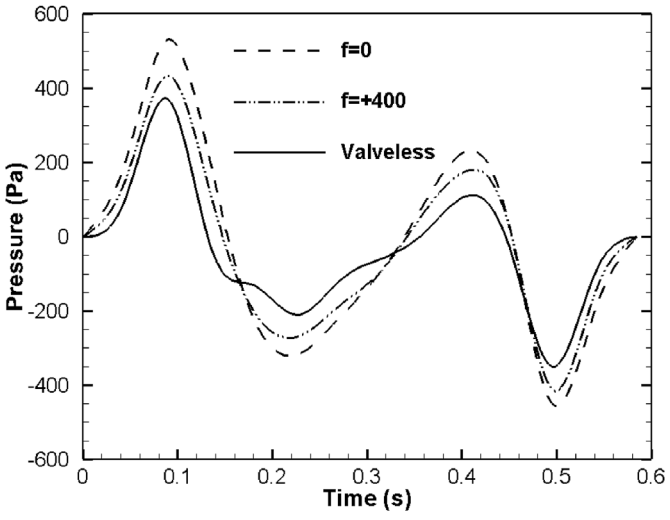

Fig. 10. Pressure difference between the MV annulus and apex during diastole for LV with valve ($f = 0$ and $f = +400$) and without valve.

Appendix A. Supplementary data

Supplementary data to this article can be found online at https://doi.org/10.1016/j.compbiomed.2018.11.024.

References

[1] S.S. Khalafvand, T.-K. Hung, E.Y.-K. Ng, L. Zhong, Kinematic, dynamic, and energy characteristics of diastolic flow in the left ventricle, Computational and Mathematical Methods in Medicine 2015 (2015) 12.
[2] R. Mittal, J.H. Seo, V. Vedula, Y.J. Choi, H. Liu, H.H. Huang, S. Jain, L. Younes, T. Abraham, R.T. George, Computational modeling of cardiac hemodynamics, J. Comput. Phys. 305 (2016) 1065–1082.
[3] J.H. Seo, V. Vedula, T. Abraham, A.C. Lardo, F. Dawoud, H. Luo, R. Mittal, Effect of the mitral valve on diastolic flow patterns, Phys. Fluids 26 (2014) 121901.
[4] B. Su, R.S. Tan, J.L. Tan, K.W.Q. Guo, J.M. Zhang, S. Leng, X. Zhao, J.C. Allen, L. Zhong, Cardiac MRI based numerical modeling of left ventricular fluid dynamics with mitral valve incorporated, J. Biomech. 49 (2016) 1199–1205.
[5] S.K. Dahl, J. Vierendeels, J. Degroote, S. Annerel, L.R. Hellevik, B. Skallerud, FSI simulation of asymmetric mitral valve dynamics during diastolic filling, Comput. Methods Biomech. Biomed. Eng. 15 (2012) 121–130.
[6] B. Su, L. Zhong, X.K. Wang, J.M. Zhang, R.S. Tan, J.C. Allen, S.K. Tan, S. Kim, H.L. Leo, Numerical simulation of patient-specific left ventricular model with both mitral and aortic valves by FSI approach, Comput. Methods Progr. Biomed. 113 (2014) 474–482.
[7] C. Chnafa, S. Mendez, F. Nicoud, Image-based large-eddy simulation in a realistic left heart, Comput. Fluids 94 (2014) 173–187.
[8] F. Domenichini, G. Pedrizzetti, Asymptotic model of fluid–tissue interaction for mitral valve dynamics, Cardiovascular Engineering and Technology 6 (2015)

95–104.
[9] S.S. Khalafvand, J.D. Voorneveld, A. Muralidharan, F.J.H. Gijsen, J.G. Bosch, T. van Walsum, A. Haak, N. de Jong, S. Kenjeres, Assessment of human left ventricle flow using statistical shape modelling and computational fluid dynamics, J. Biomech. 74 (2018) 116–125.
[10] C.T. Metz, N. Baka, H. Kirisli, M. Schaap, S. Klein, L.A. Neefjes, N.R. Mollet, B. Lelieveldt, M.d. Bruijne, W.J. Niessen, T.v. Walsum, Regression-based cardiac motion prediction from single-phase CTA, IEEE Trans. Med. Imag. 31 (2012) 1311–1325.
[11] R.I. Issa, Solution of the implicitly discretised fluid flow equation by operators-splitting, J. Comput. Phys. 62 (1986) 40–65.
[12] S.S. Khalafvand, E.Y.-K. Ng, L. Zhong, T.-K. Hung, Three-dimensional diastolic blood flow in the left ventricle, J. Biomech. 50 (2017) 71–76.
[13] S.S. Khalafvand, L. Zhong, E.Y.K. Ng, Three-dimensional CFD/MRI modeling reveals that ventricular surgical restoration improves ventricular function by modifying intraventricular blood flow, International Journal for Numerical Methods in Biomedical Engineering 30 (2014) 1044–1056.
[14] M.S. Chong, A.E. Perry, B.J. Cantwell, A general classification of three-dimensional flow fields, Phys. Fluid. Fluid Dynam. 2 (1990) 765–777.
[15] Q. Long, R. Merrifield, X.Y. Xu, P. Kilner, D.N. Firmin, G.Z. Yang, Subject-specific computational simulation of the left ventricular flow based on magnetic resonance imaging, Proc. Inst. Mech. Eng. H 222 (2007).
[16] N.R. Saber, N.B. Wood, A.D. Gosman, R.D. Merrifield, G.-Z. Yang, C.L. Charrier, P.D. Gatehouse, D.N. Firmin, Progress towards patient-specific computational flow modeling of the left heart via combination of magnetic resonance imaging with computational fluid dynamics, Ann. Biomed. Eng. 31 (2003) 42–52.
[17] T. Schenkel, M. Malve, M. Reik, M. Markl, B. Jung, H. Oertel, MRI-based CFD analysis of flow in a human left ventricle: methodology and application to a healthy heart, Ann. Biomed. Eng. 37 (2009).
[18] S.N. Doost, L. Zhong, B. Su, Y.S. Morsi, Two-dimensional intraventricular flow pattern visualization using the image-based computational fluid dynamics, Comput. Methods Biomech. Biomed. Eng. (2016) 1–16.
[19] T.B. Le, F. Sotiropoulos, On the three-dimensional vortical structure of early diastolic flow in a patient-specific left ventricle, Eur. J. Mech. B Fluid 35 (2012) 20–24.
[20] J.H. Seo, R. Mittal, Effect of diastolic flow patterns on the function of the left ventricle, Phys. Fluids 25 (2013) 110801.
[21] V. Vedula, S. Fortini, J.-H. Seo, G. Querzoli, R. Mittal, Computational modeling and validation of intraventricular flow in a simple model of the left ventricle, Theor. Comput. Fluid Dynam. 28 (2014) 589–604.
[22] M.S.M. Elbaz, E.E. Calkoen, J.J.M. Westenberg, B.P.F. Lelieveldt, A.A.W. Roest, R.J. van der Geest, Vortex flow during early and late left ventricular filling in normal subjects: quantitative characterization using retrospectively-gated 4D flow cardiovascular magnetic resonance and three-dimensional vortex core analysis, J. Cardiovasc. Magn. Reson. 16 (2014) 78.